CHARACTERISATION OF THE ANGULAR MOMENTUM TRANSPORT IN ASDEX

A. Kallenbach, H. M. Mayer,
G. Fussmann, V. Mertens, U. Stroth, O. Vollmer
and the ASDEX Team

IPP I/255 October 1990

MAX-PLANCK-INSTITUT FÜR PLASMAPHYSIK

8046 GARCHING BEI MÜNCHEN

MAX-PLANCK-INSTITUT FÜR PLASMAPHYSIK

GARCHING BEI MÜNCHEN

CHARACTERISATION OF THE ANGULAR MOMENTUM TRANSPORT IN ASDEX

A. Kallenbach, H. M. Mayer,
G. Fussmann, V. Mertens, U. Stroth, O. Vollmer
and the ASDEX Team

IPP I/255 October 1990

Die nachstehende Arbeit wurde im Rahmen des Vertrages zwischen dem Max-Planck-Institut für Plasmaphysik und der Europäischen Atomgemeinschaft über die Zusammenarbeit auf dem Gebiete der Plasmaphysik durchgeführt.

Characterisation of the Angular Momentum Transport in ASDEX

A. Kallenbach, H.M. Mayer, G. Fussmann, V. Mertens, U. Stroth O. Vollmer
and the ASDEX Team

Max-Planck-Institut für Plasmaphysik
D–8046 Garching, Federal Republic of Germany
EURATOM–IPP Association

October 1, 1990

Abstract

Angular momentum transport studies were conducted for nearly stationary situations of about 50 neutral-beam-heated ASDEX discharges under a variety of experimental conditions. Comparison of the confinement times of angular momentum and energy reveals close similarities between thermal and perpendicular momentum transport. Scaling laws are derived for the dependence of the central rotation speed, the momentum confinement time and the radially averaged momentum diffusivity from the main experimental parameters of L-mode discharges. The L-mode results are compared with the momentum transport behaviour during the improved confinement phase of H-mode, pellet-fuelled and counter-NI discharges.

1 Introduction

The investigation of the toroidal rotation velocity attained during neutral beam heating provides further insight into the general problem of confinement and transport in tokamaks. Many tokamaks have reported similar magnitudes and dependences on individual plasma parameters of the energy confinement time τ_E and the angular momentum confinement time τ_ϕ (SUCKEWER

et al., 1981), (BRAU *et al.*, 1983), (ISLER *et al.*, 1986), (BURRELL *et al.*, 1988), (ST. JOHN *et al.*, 1989), (WEISEN *et al.*, 1989), (SCOTT *et al.*, 1990b), (KALLENBACH *et al.*, 1990). Since the classical perpendicular viscosity is far too low to explain the observed rotation damping (CONNOR *et al.*, 1987), an anomalous transport mechanism is believed to cause the radial transport of momentum which is a feature of the ions alone owing to the low mass of the electrons. The correlation of energy and momentum confinement can be taken as indicating the existence of a common transport mechanism for thermal conduction and momentum diffusion. There is also some evidence from theory to support this assumption, e.g., the ion-temperature-gradient driven class of instabilities produces equal ion heat and momentum diffusivities ($\chi_i = \chi_\phi$) (MATTOR and DIAMOND, 1988). A neoclassical attempt to describe the high momentum losses by means of the gyroviscosity (STACEY and SIGMAR, 1985) has recently become the subject of controversial discussion in this journal (STACEY, 1989), (CONNOR *et al.*, 1989).

For comparison of experiment with theory, particularly the dependence of momentum transport on experimental parameters such as the density, current or heating power may serve as a useful test. Many theories should be able to predict these dependences more accurately than the absolute value of the effective momentum flux.

This paper gives a comprehensive characterisation of the momentum transport behaviour in ASDEX. The experimental setup and data evaluation procedure used to derive momentum confinement properties are described in Section 2. Scaling laws for the dependence on experimental parameters of neutral-beam-heated L-mode discharges are presented in Section 3. The behaviour of momentum transport during discharges with improved confinement properties is discussed in Section 4. A summary of the results is given in Section 5.

2 Experimental procedure and data evaluation

Toroidal rotation velocities are measured simultaneously at 5 radial positions in the outer plasma half-plane by means of charge exchange recombination (CXR) spectroscopy. The spectra of O^{VIII} or C^{VI} lines excited by CXR with NI heating beam neutrals are taken with a 50 ms repetition frequency. A detailled description of the experimental setup and the geometrical arrangement is given by (KALLENBACH *et al.*, 1990). Velocities measured with deuterium injection are corrected by typically 10 % in order to compensate the effect of the energy dependence of the CXR rate coefficients on the Doppler-broadened spectral line shapes (HOWELL *et al.*, 1988). In

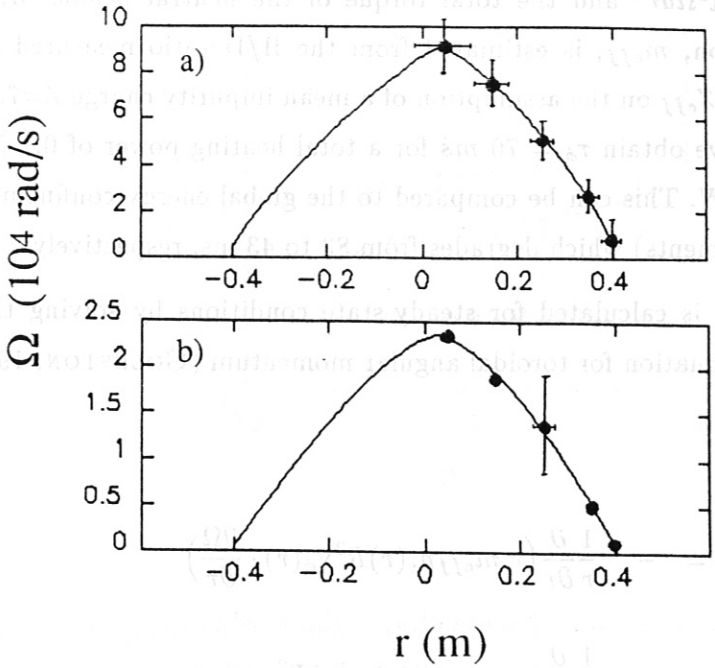

Figure 1: *Measured angular rotation frequencies for a discharge with two different neutral injection power levels. The curves represent analytic fits to the measured values on the assumption of a constant rotation frequency on a flux surface. The horizontal error bars displayed in a) represent the full radial half-widths of the beam neutrals along the corresponding line of sight.* $I_p = 0.42\ MA$; $\overline{n}_e = 4.6 \cdot 10^{19}\ m^{-3}$ *a)* $P_{NI} = 1.8MW$, *b)* $P_{NI} = 0.3MW$.

the case of hydrogen injection, no correction was necessary for the ASDEX NI beam parameters owing to the small energy dependence of the rate coefficients at the higher beam velocities.

For further analysis the rotation velocities are converted into angular rotation frequencies and fitted to a smooth analytical function on the assumption of constant rotation frequency on a flux surface (BURRELL *et al.*, 1988). The toroidal rotation velocity of all plasma ions is assumed to be equal to the velocity of the measured impurity species owing to the fast momentum exchange between ions of different types. As an example, measured data points and the corresponding flux surface fits for a discharge with two different neutral injection power levels are shown in Fig. 1.

The global momentum confinement time τ_ϕ is calculated as the ratio of the total plasma angular

momentum $L_\phi = \int m_{eff} n_e R^2 \Omega dr^3$ and the total torque of the neutral beams M_{tot}. The mean plasma mass per electron, m_{eff}, is estimated from the H/D ratio measured by mass spectrometry and an averaged Z_{eff} on the assumption of a mean impurity charge Z=7. For the example displayed in Fig. 1, we obtain $\tau_\phi = 70\ ms$ for a total heating power of 0.7 MW and $\tau_\phi = 42\ ms$ for $P_{tot} = 1.95$ MW. This can be compared to the global energy confinement time τ_E (from diamagnetic measurements) which degrades from 83 to 43 ms, respectively.

The momentum diffusivity χ_ϕ is calculated for steady-state conditions by solving the time-independent radial transport equation for toroidal angular momentum (GOLDSTON, 1985):

$$\begin{aligned} M_b(r,\Omega) = & - \frac{1}{r}\frac{\partial}{\partial r}\Big(r\ m_{eff} n_e(r) R^2 \chi_\phi(r) \cdot \frac{\partial \Omega}{\partial r}\Big) \\ & + \frac{1}{r}\frac{\partial}{\partial r}(r\ m_{eff} n_e(r) v_r(r) R^2 \cdot \Omega) \\ & + \frac{n_e(r) m_{eff}}{\tau_{\phi,CX}(r)} R^2 \cdot \Omega \end{aligned} \qquad (1)$$

The torque density M_b is calculated by employing the simplifying assumption that the torque is delivered at the flux radius where ionisation occurs (KALLENBACH *et al.*, 1990). The second term on the right-hand side of Eq. 1 describes the convection of momentum with the radial plasma flow velocity v_r, which balances the effect of beam fuelling for steady-state conditions. The third term in Eq. 1 with the phenomenological loss time $\tau_{\phi,cx}$ (GOLDSTON, 1985) takes into account the momentum loss due to charge exchange with background neutrals which affects the momentum transport near the edge. For the plasma conditions relevant to this paper, the inclusion of the convective and charge exchange momentum loss terms leads only to small changes in the calculated momentum diffusivity χ_ϕ in the plasma bulk.

Momentum diffusivities χ_ϕ calculated for the discharge of Fig. 1 are shown in Fig. 2. It can be clearly seen that the transport of momentum is reduced over the whole plasma cross-section for the lower heating power condition.

In the following, the momentum diffusivity χ_ϕ is used in terms of a radially averaged $\overline{\chi}_\phi$ which has a higher accuracy than the local values. The average is taken between r=8 cm and r=34 cm. For $r < 8\ cm$, the small gradients in Ω produces large errors in χ_ϕ so that the calculated

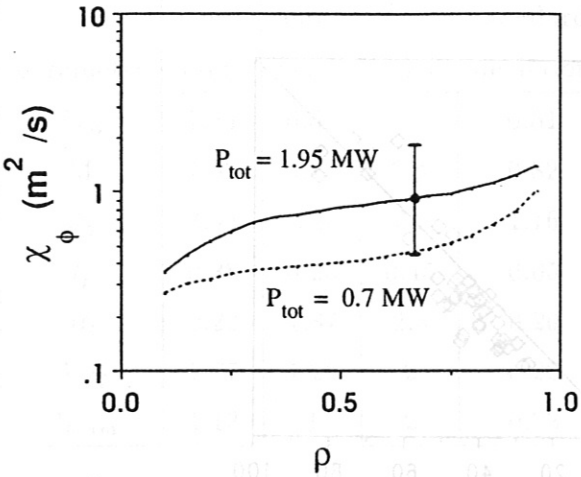

Figure 2: χ_ϕ *versus normalized flux coordinate* ρ *for the two power levels* $P_{tot} = P_{NI} + P_{OH}$ *of the discharge shown in Fig. 1. The radially averaged* $(8 < r < 34\ cm)$ *values of* $\overline{\chi}_\phi$ *are 0.45 and 0.85* m^2/s*, respectively.*

value mainly depends on the fitting function used for $\Omega(r)$. Near the edge, the larger relative experimental error of the velocity in combination with the not very well-known charge exchange loss term leads to high uncertainties in the local χ_ϕ .

In order to obtain information about the variation of momentum confinement with the plasma parameters, we built up a data base including the momentum transport analysis results for about 50 ASDEX discharges under various experimental conditions. Care was taken to ensure that the momentum transport under investigation was not disturbed by MHD mode-locking events, which can serve as a very effective momentum loss term (ZOHM *et al.*, 1990). A comparison of the global momentum confinement times τ_ϕ with the corresponding energy confinement time τ_E for co-NI, L-mode conditions is shown in Fig. 3. The similar magnitude of the two values over the whole data range is a clear indicator of the existence of a (partly) common transport mechanism for momentum and energy. However, in the region of lower confinement times τ_ϕ is systematically lower than τ_E.

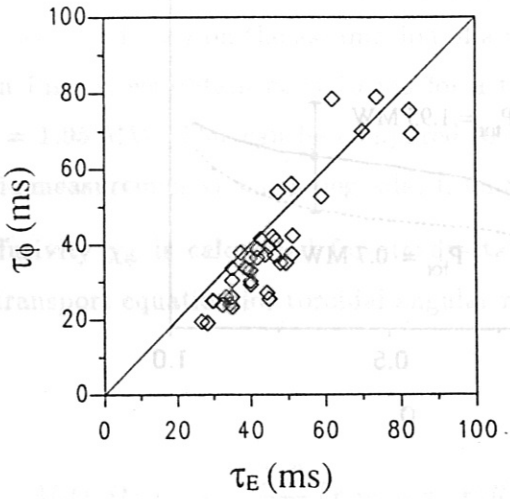

Figure 3: *Comparison of the angular momentum confinement time τ_ϕ with the energy confinement time τ_E for different experimental parameters.*

3 Scaling laws

3.1 Transport properties

We derived scaling laws for the dependence of momentum transport properties on the main plasma parameters for co-NI, L-mode conditions by applying the SAS code (SAS, 1985). For simplicity we used ordinary least-squares fits after a logarithmic transformation. The experimental parameter range covered by the analysis is described in Table 3.1.

The uncertainty of the regression coefficients is typically ± 0.05 for P_{tot} and $\overline{n}_e$ and ± 0.15 for the other quantities. Parameters with exponential dependences of less than 0.15 were omitted as fitting parameters. The total power P_{tot} and the torque of the neutral beams, M, were only used alternatively in the least-squares fitting procedure since they are highly correlated. For velocity scalings we preferred the driving term M and for the scaling of confinement properties we took the total power, which is more directly connected with transport enhancement. Z_{eff} was excluded from the analysis since no significant dependence of any momentum transport property on this quantity was found. All discharges were carried out in divertor configuration with a plasma radius of a = 40 cm.

exp. parameter	mean value	min. value	max. value	standard deviation	unit
P_{tot}	1.44	0.58	2.3	0.51	MW
M	1.52	0.22	3.4	0.82	Nm
$\overline{n}_e$	3.43	1.6	7.6	1.16	$10^{19}\ m^{-3}$
I_p	0.38	0.25	0.45	0.05	MA
B_t	2.22	1.87	2.8	0.26	T
A_{eff}	1.77	1.26	2	0.22	amu
A_{beam}	1.13	1	2	0.33	amu

Table 1: Description of the experimental parameter range covered by statistical analysis.

A very simple expression is obtained for the central rotation velocity v_0:

$$v_0 \;=\; 29.4 \cdot \left(\frac{M}{\overline{n}_e}\right)^{\mathbf{0.61}} \cdot I_p^{\mathbf{0.3}} \qquad (10^4\ m/s,\ Nm,\ 10^{19}\ m^{-3},\ MA). \quad (2)$$

The central speed is approximately independent of B_t and the mean plasma mass number per electron, A_{eff}, indicating a nearly linear isotope effect for the central angular momentum. The current dependence of v_0 is weak. Figure 4 demonstrates the good reproduction of the measured velocities by the simple scaling law of Eq. 2 over the whole parameter range. The scaling obtained for the momentum confinement time is given in Eq. 3. The corresponding τ_E scaling of the data base is given in Eq. 4 for comparison:

$$\tau_\phi \;=\; 36 \cdot P_{tot}^{\mathbf{-0.7}} \cdot \overline{n}_e^{\mathbf{0.45}} \cdot I_p^{\mathbf{0.85}} \cdot A_{eff}^{\mathbf{1.0}} \cdot A_{beam}^{\mathbf{-0.2}} \cdot \left(\frac{B_t}{2.2}\right)^{\mathbf{-0.8}}, \quad (3)$$

$$\tau_E \;=\; 37 \cdot P_{tot}^{\mathbf{-0.58}} \cdot \overline{n}_e^{\mathbf{0.35}} \cdot I_p^{\mathbf{0.5}} \cdot A_{eff}^{\mathbf{0.65}} \qquad (ms,\ MW,\ 10^{19}\ m^{-3},\ MA,\ amu,\ T). \quad (4)$$

The scaling for the radially averaged $\overline{\chi}_\phi$ $(8 < r < 34\ cm)$ reads

$$\overline{\chi}_\phi \;=\; 1.69 \cdot P_{tot}^{\mathbf{0.65}} \cdot \overline{n}_e^{\mathbf{-0.73}} \cdot I_p^{\mathbf{-0.65}} \cdot A_{eff}^{\mathbf{-0.8}} \qquad (ms,\ MW,\ 10^{19}\ m^{-3},\ MA,\ amu). \quad (5)$$

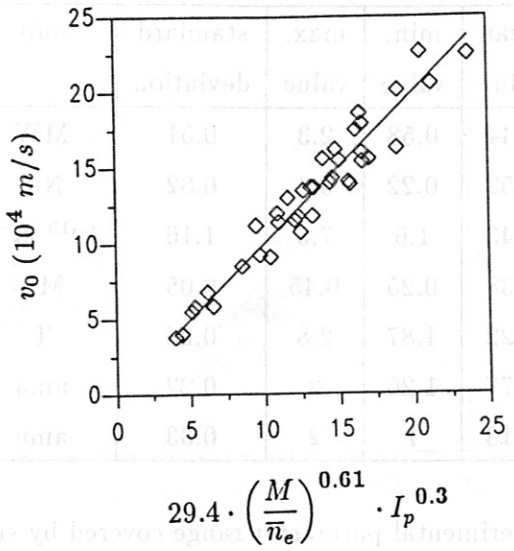

Figure 4: *Measured central rotation velocity v_0 versus the prediction of the scaling law of Eq. 2.*

The close correlation between energy and momentum transport is obvious. Remarkable is the well developed isotope dependence of τ_ϕ and $\overline{\chi}_\phi$. The slightly degraded momentum confinement with deuterium injection is possibly due to the less favourable torque deposition profile owing to the higher beam stopping cross-section. The outward shift of the beam deposition profile for high-density discharges may also explain the weaker density dependence of τ_ϕ in comparison with $\overline{\chi}_\phi$. The more favourable current dependence of τ_ϕ in comparison with v_0 stems from a broadening of the velocity profile with increasing current. A quite astonishing feature is the B_t dependence of τ_ϕ, which is not observed in τ_E and $\overline{\chi}_\phi$. This effect will be discussed in the next section.

To give an impression of the scatter of the experimental results around the scaling law of Eq. 5, Fig. 5 shows the experimentally determined diffusivity $\overline{\chi}_\phi$ versus the predicted value. The scaling tends slightly to overestimate χ_ϕ for extremely high and low-power shots. The reason for this behaviour is the imperfect description of the power dependence of χ_ϕ by the power law throughout the whole power range involved. The variation of momentum content with injected power seems to be partly of an offset-linear type.

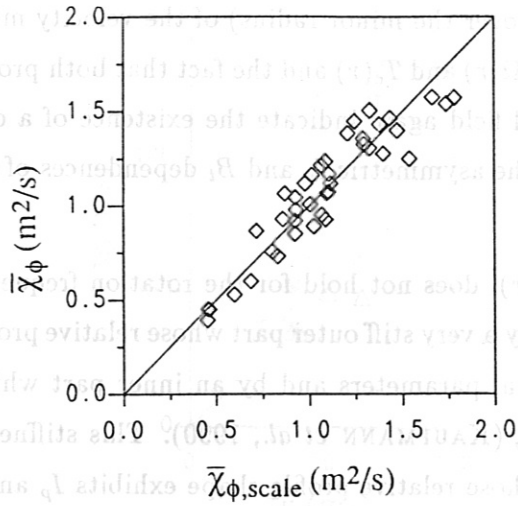

Figure 5: *Measured radially averaged momentum diffusivity* $\overline{\chi}_\phi$ *(8 cm* $< r <$ *34 cm) versus the prediction of the scaling law of Eq. 5.*

3.2 Profile shapes

An often used quantity for the characterisation and discussion of profile shapes is the peaking factor Q, the ratio of the central to the volume-averaged value. The regression analysis for L-mode conditions obtains the following peaking factor scaling for the angular rotation frequency and, for reference, the electron temperature and density:

$$Q_\Omega = 2.3 \cdot (I_p/0.38)^{-0.45} \cdot (B_t/2.2)^{0.95} \qquad (MA,\ T), \tag{6}$$

$$Q_{Te} = 2.3 \cdot (I_p/0.38)^{-0.7} \cdot (B_t/2.2)^{0.7} \qquad (MA,\ T), \tag{7}$$

$$Q_n = 1.6 \cdot (I_p/0.38)^{-0.35} \cdot (B_t/2.2)^{0.35} \qquad (MA,\ T), \tag{8}$$

where I_p and B_t have been normalized to their mean values to facilitate an easier comparison. The safety factor variation in the data base is $2 < q_a < 4$ leading to $2 < Q_\Omega < 3.1$, $1.8 < Q_t < 2.9$ and $1.3 < Q_n < 1.8$. The dependence of $Q_{\Omega,\ Te,\ n}$ on other experimental parameters is small and has been omitted in the regression analysis.

A detailed comparison of electron temperature and angular velocity profile shapes suffers from the rather poor resolution (5 points over the minor radius) of the velocity measurement. However, the quite similar peakedness of $\Omega(r)$ and $T_e(r)$ and the fact that both profile shapes depend only on the current and the toroidal field again indicate the existence of a common transport mechanism. The main difference is the asymmetric I_p and B_t dependences of Q_Ω, i.e. Q_Ω is not a pure function of q_a.

Profile stiffness, as observed for $T_e(r)$, does not hold for the rotation frequency: The electron temperature profile is characterised by a very stiff outer part whose relative profile shape depends only very weakly on the experimental parameters and by an inner part which is strongly q_a-dependent (MURMANN *et al.*, 1986), (KAUFMANN *et al.*, 1990). This stiffness is not observed for the rotation frequency profile, whose relative profile shape exhibits I_p and B_t dependences over the whole minor radius.

For a further investigation of the origin of the B_t dependence of τ_ϕ and its absence for $\overline{\chi}_\phi$, we also derived a scaling law for the local toroidal velocity at r = 35 cm:

$$v_{35} \;=\; 50 \cdot \left(\frac{M}{\overline{n}_e}\right)^{\mathbf{0.55}} \cdot {I_p}^{\mathbf{1.0}} \cdot {B_t}^{\mathbf{-1.6}} \qquad (10^4\ m/s,\ 10^{19}\ m^{-3},\ Nm,\ MA,\ T). \quad (9)$$

Only the dominant parameters were taken into account since the relative scatter of the measured near-edge velocities is quite large. The scaling law of Eq. 9 indicates a strong q_a dependence of the near-edge rotation velocity as well as considerably increased momentum losses for higher toroidal fields. In fact, the observed B_t dependence of the global τ_ϕ is exclusively caused by this strong B_t dependence of the edge momentum transport. The global momentum confinement time for radii $r < 35\ cm$ is found to be independent of the toroidal field. The lack of a B_t dependence of $\overline{\chi}_\phi$ as given in Eq. 5 is simply due to the exclusion of the near-edge region from $\overline{\chi}_\phi$.

The physical origin of the B_t dependence of the near-edge momentum transport is still unclear and will be the subject of further studies.

4 Momentum transport of regimes with improved confinement

After the detailed characterisation of the L-mode confinement behaviour, we now turn to the regimes of improved confinement obtained during neutral injection on ASDEX. We concentrate

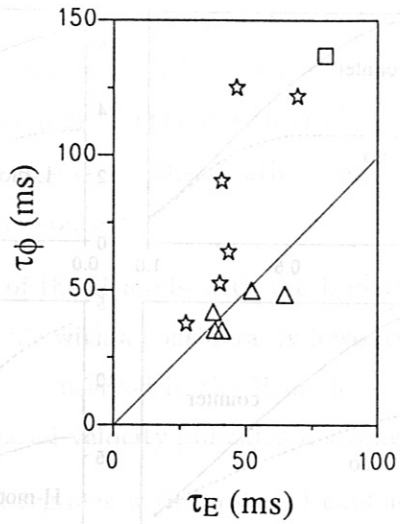

Figure 6: *Angular momentum confinement time τ_ϕ versus energy confinement time τ_E for discharges with improved confinement conditions.*
Triangles: H-mode; stars: counter-NI; square: pellet fuelling.

on the qualitative changes during counter-NI, pellet-fuelled and H-mode discharges. As an overview, Fig. 6 shows a comparison of the global confinement times τ_ϕ and τ_E. For discharges with peaked density profiles (pellet-fuelled and counter-NI), the confinement improvement is much more distinct in τ_ϕ than in τ_E. This behaviour indicates that primarily the ion transport is improved. In contrast to this, H-mode discharges exhibit comparable improvement of momentum and energy confinement.

In order to demonstrate the momentum transport behaviour of discharges with improved confinement, Fig. 7 compares the density profiles, rotation frequency profiles and χ_ϕ profiles of a pellet-fuelled, a counter-NI and and a quiescent H-mode discharge with those of discharges with nearly identical external experimental parameters (The power levels are different in the various improved confinement modes). The discharges chosen for Fig. 7 are typical examples and are backed up by similar ones to make due allowance for the large error bars of our local χ_ϕ calculation owing to the experimental scatter of a single rotation profile measurement. The calculation of χ_ϕ (r) was done by means of Eq. 1, charge exchange effects and time derivatives being neglected for simplicity.

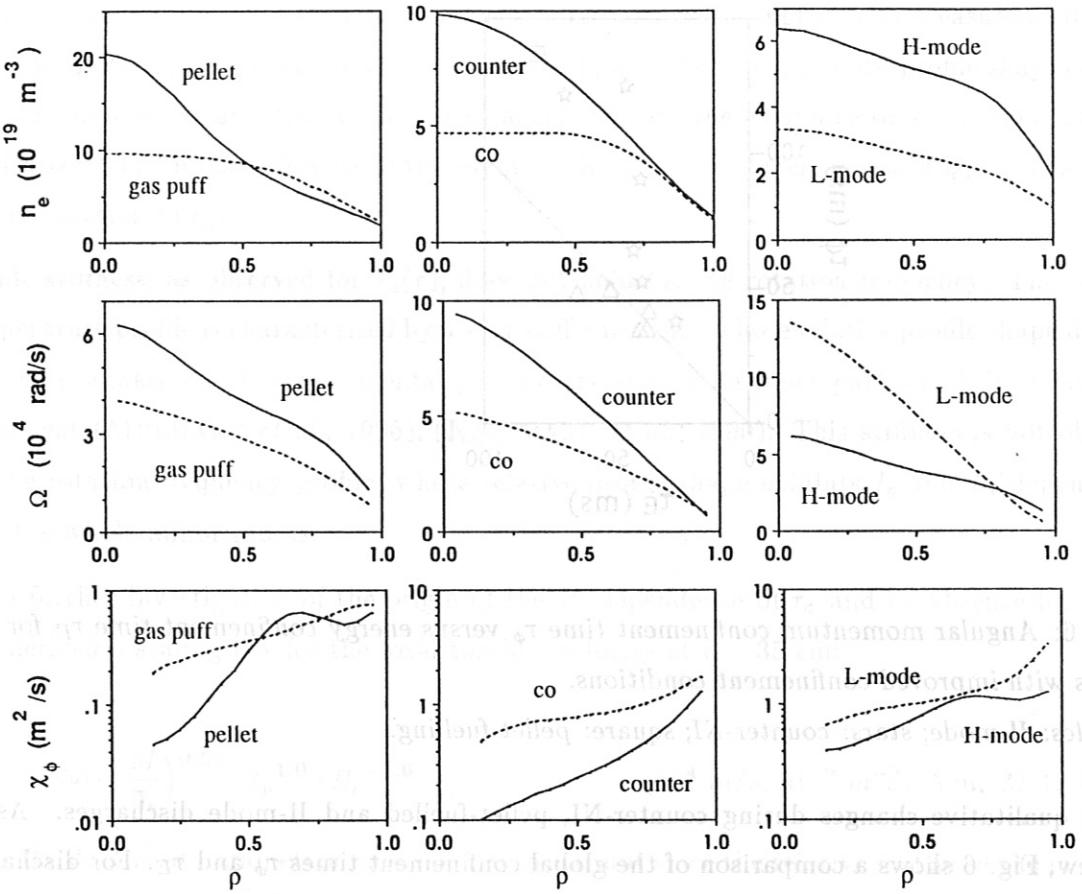

Figure 7: *Characterisation of the changes in momentum transport for discharges with improved confinement conditions. The solid lines show the profiles of electron density, angular rotation frequency and momentum diffusivity during a pellet-fuelled discharge, a counter-NI heated discharge and a co-NI discharge with a quiescent H-mode. The corresponding profiles for standard co-NI, L-mode discharges with similar experimental parameters are given for comparison as dotted lines.*

L-mode versus pellet-fuelled: $P_{NI} = 0.76\ MW$, $I_p = 0.42\ MA$, $B_t = 2.2\ T$, $\overline{n}_e = 7.6 \rightarrow 10.4\ 10^{19}\ m^{-3}$, $\tau_\phi = 78 \rightarrow 137$ *ms*, $\tau_E = 62 \rightarrow 80$ *ms.*

co versus counter-NI: $P_{NI} = 0.9\ MW$, $I_p = 0.42\ MA$, $B_t = 2.0\ T$, $\overline{n}_e = 4 \rightarrow 6.4\ 10^{19}\ m^{-3}$, $\tau_\phi = 42 \rightarrow 120$ *ms*, $\tau_E = 50 \rightarrow 70$ *ms.*

L-mode versus H-mode: $P_{NI} = 2.4\ MW$, $I_p = 0.42\ MA$, $B_t = 2.6\ T$, $\overline{n}_e = 2.6 \rightarrow 5.1\ 10^{19}\ m^{-3}$, $\tau_\phi = 26 \rightarrow 49$ *ms*, $\tau_E = 35 \rightarrow 65$ *ms.*

The two types of discharges with peaked density profile show rather similar behaviour: The momentum transport is strongly reduced in the plasma centre and is nearly unchanged close to the edge. The best confinement is achieved after complete suppression of sawteeth when the density peaking is at maximum (KALLENBACH *et al.*, 1990). Although the density is higher than in the corresponding L-mode cases, the rotation frequency is significantly increased, leading to a much higher momentum content.

In contrast, comparison of the H-mode with the L-mode case reveals a higher H-mode density, but a flatter rotation profile with a considerably lower central rotation speed. The improvement of momentum confinement observed in the H-mode has its origin mainly in the region close to the edge, where an increased velocity indicates a strongly reduced momentum transport.

A common feature of all regimes with improved confinement investigated here is the fact that the velocity rise always appears at the same radial position where the density gradient steepens.

5 Summary and conclusions

We derived scaling laws for the dependence of different momentum transport properties on the main experimental parameters under L-mode conditions, using statistical analysis. The comparison of absolute values as well as the power law coefficients obtained for the global confinement times τ_ϕ and τ_E yield close similarities between energy and momentum transport. The main difference in the transport behaviour appears in the B_t dependence observed for the momentum confinement time. This dependence can be attributed to enhanced angular momentum losses near the plasma edge with increasing toroidal field. The bulk momentum transport does not depend on B_t. However, the physical origin (and its lacking influence on energy transport) of these increased losses has to be the subject of further studies.

The peaking factor Q_Ω of the angular rotation frequency is a function of the current and toroidal magnetic field alone. But unlike Q_{Te} and Q_n, Q_Ω is not simply q_a-dependent. The degradation of the outer part of the rotation profile with increasing toroidal field is more distinct than the growing effect of the increasing plasma current.

Analysis of discharges with improved confinement behaviour reveals clear differences between regimes with peaked density profiles and the H-mode: In the counter-NI and pellet-fuelled regimes, the improvement of τ_ϕ is much more pronounced than the improvement of τ_E, indicating

a change predominantly in ion transport. The changes in transport occur in the inner part of the plasma. On the other hand, the improvements in τ_ϕ and τ_E during the H-mode are of the same order of magnitude and the reduction in momentum transport is mainly located near the separatrix.

Generally, the reduction of momentum transport for discharges with improved confinement is localized in that radial region where the density profile shape steepens. It cannot be decided from our experimental data whether this is caused by changes in a scale length, e.g., η_i, or it is a simple coincidence owing to the fact that particle and momentum transport have the same underlying reason.

The results of our regression analysis (Eq. 3) can be compared with the prediction of the neoclassical gyroviscous theory $\tau_{\phi,\,gyro} \approx 2 \cdot R_0^2 BZe/\overline{T}$ (STACEY and SIGMAR, 1985). There is clear disagreement in the B_t, I_p and A_{eff} dependences.

At last, the nature of momentum transport seems to be anomalous to a high extent. This shows up in the isotope effect appearing almost linearly in the L-mode scaling as well as in the drastic variations in χ_ϕ during discharges with peaked density profiles which will need nonlinear mechanisms as an explanation. The close correlation of τ_ϕ and τ_E over a broad range of experimental parameters and the similar scaling favours those theories of anomalous transport predicting equal ion thermal and momentum loss rates. Recently, a direct comparison of χ_ϕ and χ_i for a limited parameter range on TFTR (SCOTT *et al.*, 1990a) revealed the relationship $\chi_\phi \approx \chi_i$ across the confinement zone.
The need to explain both ion thermal and momentum transport by one mechanism may help to reduce the well-stocked 'zoo' of anomalous transport theories.

References

Brau, K., Bitter, M., Goldston, R. J., Manos, D., McGuire, K., and Suckewer, S. (1983). *Nucl. Fusion* **23**, 1643–1655.

Burrell, K. H., Groebner, R. J., St. John, H., and Seraydarian, R. P. (1988). *Nucl. Fusion* **28**, 3–15.

Connor, J. W., Cowley, S. C., and Hastie, R. J. (1989). *Plasma Phys. Controlled Fusion* **31**, 1469–1475.

Connor, J. W., Cowley, S. C., Hastie, R. J., and Pan, L. R. (1987). *Plasma Phys. Controlled Fusion* **29**, 919–931.

Goldston, R. (1985). *in Basic Physical Processes of Toroidal Fusion Plasmas (Proc. Course and Workshop Varenna, 1985), Vol. 1, CEC, Luxembourg* , 165–186.

Howell, R. B., Fonck, R. J., Knize, R. J., and Jaehnig, K. P. (1988). *Rep. PPPL-2539, Princeton Plasma Physics Laboratory, NJ* .

Isler, A. J. *et al.* (1986). *Nucl. Fusion* **26**, 391–413.

Kallenbach, A., Mayer, H. M., Fussmann, G., Büchse, R., Gruber, O., Klüber, O., Mertens, V., Vollmer, O., and Zohm, H. (1990). *Nucl. Fusion* **30**, 645–656.

Kaufmann, M., Sandmann, W., Bessenrodt-Weberpals, M., Büchl, K., Gruber, O., Kardaun, O., Lackner, K., Lang, R., Mertens, V., Murmann, H., Neuhauser, J., and Söldner, F. (1990). *Plasma Phys. Controlled Fusion* **32**, 303–308.

Mattor, N. and Diamond, P. H. (1988). *Phys. Fluids* **31**, 1180–1189.

Murmann, H., Wagner, F., *et al.* (1986). *in Controlled Fusion and Plasma Heating (Proc. 13th Eur. Conf. Schliersee, 1986), Vol. 10C, Part I, European Physical Society* , 216–219.

SAS (1985). *User's Guide: Statistics.* SAS Institute Inc., Cary, North Carolina, U.S.A.

Scott, S. D. *et al.* (1990a). *Phys. Fluids B* **2**, 1300–1305.

Scott, S. D. *et al.* (1990b). *Phys. Rev. Lett.* **64**, 531–534.

St. John, H., Stroth, U., Burrell, K. H., Groebner, R., DeBoo, J., and Gohil, P. (1989). *in Controlled Fusion and Plasma Physics (Proc. 16th Eur. Conf. Venice, 1989), Vol. 12B, Part I, European Physical Society* , 119–122.

Stacey, W. M. (1989). *Plasma Phys. Controlled Fusion* **31**, 1451–1468.

Stacey, W. M. and Sigmar, D. J. (1985). *Phys. Fluids* **28**, 2800–2807.

Suckewer, S., Eubank, H. P., Goldston, R. J., McEnerney, J., Sauthoff, N. R., and Towner, H. H. (1981). *Nucl. Fusion* **21**, 1301–1309.

Weisen, H., von Hellermann, M., Boileau, A., Horton, L. D., Mandl, W., and P., S. H. (1989). *Nucl. Fusion* **29**, 2187–2197.

Zohm, H., Kallenbach, A., Bruhns, H., Fussmann, G., and Klüber, O. (1990). *Europhys. Lett.* **11**, 745–750.